



Cite this: *J. Mater. Chem. C*, 2016, 4, 5814

A novel paradigm for the fabrication of highly uniform nanowire arrays using residual stress-induced patterning†

Zhi Zhao,^a Nan Wang,^b Hanqing Nan,^a Li Shen,^a Colm Durkan^b and Ximin He^{*ac}

Patterned low-dimensional (1-D or 2-D) nanomaterials have recently drawn tremendous attention due to their unique properties. To realize their wide range of potential applications in electronics, sensing and energy storage, it is critical yet still challenging to fabricate highly uniform 1-D material arrays (e.g. nanowire arrays) that simultaneously feature high resolution, large scale and tunable geometric parameters. Herein, we report a novel method for the fabrication of large-area, highly aligned nanowire arrays using the combination of one-step residual-free nanopatterning *via* pressure-induced instabilities and low-temperature hydrothermal synthesis. We demonstrate that the fabrication of highly tunable, vertically aligned single-crystal zinc oxide (ZnO) nanowire (NW) arrays can be achieved on arbitrary substrates. The height, diameter, locations and orientations of ZnO NWs are precisely controlled through the spatial confinement effect of the spontaneously formed polymer masks. The high qualities of the as-prepared NW arrays have been revealed by the systematic characterization of the morphology, crystallinity, and electronic properties of single ZnO NWs. Conductive atomic force microscopy (cAFM) measurements show Schottky barrier characteristics in the *I*-*V* curves and a clear registration of the detected current signal with individual NWs. Mechanically-induced currents are observed to change with the deformation magnitude of NW, directly indicating the generation of piezoelectricity. This work provides a novel universal paradigm for patterned 1-D nanomaterial fabrication and opens up unprecedented opportunities for more design innovations and applications in nano-devices.

Received 22nd April 2016,
Accepted 23rd May 2016

DOI: 10.1039/c6tc01653g

www.rsc.org/MaterialsC

Introduction

Nanomaterials such as one-dimensional metal (oxide) nanowires or two-dimensional atomic layers have been identified as useful building blocks for nanoscale electronic devices, when they are grown or aligned in a controlled structure.^{1–4} Zinc oxide (ZnO) nanowires (NWs), for example, have attracted extensive research interest because of their semiconducting-piezoelectric dual properties,⁵ direct bandgap and large exciton binding energy,^{6,7} and the diversity of synthetic and processing strategies.⁸ ZnO NWs grown perpendicular to the substrate with uniform morphology and good alignment are particularly useful in applications including antireflection optics, ZnO-polymer hybrid photovoltaic devices, and chemical/biochemical sensors.^{9–11} The foremost

promising application of ZnO NWs in piezoelectricity generators is based on large-area highly-aligned arrays of piezoelectric NWs, which convert mechanical energy into electrical energy when they are uniaxially compressed.^{12,13} Thus the controlled growth of well-aligned nanomaterials in predetermined configurations is the critical prerequisite for realizing the advanced functions of many 1-D materials.^{14–21} In particular, the morphology control of NW materials includes NW shape, diameter, height and crystallinity, as well as the arrangement of NW arrays, such as the periodicity and symmetry of NW arrays. Consequently, there is a strong demand for nanopatterning schemes compatible with a wide variety of geometric parameters and device fabrication processes.²²

Wet chemical synthetic routes to many metal oxide NWs at low temperature (<100 °C) are favorable for their compatibility with broad choices of substrates and electronics manufacturing in comparison with high-temperature (>600 °C) vapor-liquid-solid (VLS) growth methods,^{23–26} but the diameter and orientation of the as-grown NWs vary significantly.²⁷ Therefore, several patterning methods have been employed to confine the NW growth *via* masking. For example, a patterned photoresist has been used to define nucleation regions to produce single crystal ZnO disks of

^a School for Engineering of Matter, Transport and Energy, Arizona State University, Tempe, AZ 85281, USA. E-mail: ximin.he@asu.edu

^b The Nanoscience Centre, University of Cambridge, 11 J. J. Thomson Avenue, Cambridge CB3 0FF, UK

^c The Biodesign Institute, Molecular Design and Biomimetics Center, Arizona State University, Tempe, AZ 85281, USA

† Electronic supplementary information (ESI) available. See DOI: 10.1039/c6tc01653g

4 μm width with an aspect ratio <0.5 , which as the building blocks created light emitting diodes and UV photovoltaic cells.²⁸ Recently, wafer-scale aligned NWs have been fabricated with polymer masks patterned by laser-interference lithography.^{29,30} Moreover, electron beam lithography (EBL) has been used to produce well-aligned patterned ZnO nanowire arrays.³¹ A common issue in those methods is the potential contamination from the post-development residue on substrates,³² which may affect the uniformity of NW alignment. Meanwhile, lack of tunability is another drawback of those methods, in which only one pattern can be generated from each photomask. In addition, the patterning resolution is limited for photolithographic methods, while EBL is not feasible for economic large-scale fabrication. The current challenge is how to develop a residue-free, tunable mask fabrication technique that simultaneously satisfies the resolution and large-scale requirement in ZnO NW synthesis.

We previously reported a non-conventional nanopatterning technique based on pressure-induced instabilities in polymer thin films.³³ Herein, we have employed this technique to synthesize highly uniform, vertically aligned ZnO NWs at nanometer resolution. In contrast to conventional lithography techniques, our method is able to produce patterns with residual-free surfaces in a single step. By controlling the patterning parameters or applying post-thermal annealing, the surface pattern sizes can be tuned between ~ 20 nm and hundreds of nm. Using this technique, we have demonstrated that ZnO NWs of various sizes can be prepared from a single stamp. The as-prepared ZnO NWs showed characteristic semiconducting-piezoelectric dual properties and promises for future electronic applications. As our method obviates the subsequent etching or developing steps required in other lithography techniques, which significantly simplifies the fabrication process and reduces the cost, we believe this strategy

provides a universal, cost-effective paradigm applicable to many other nanomaterials.

Experimental

Polymer mask fabrication

A detailed polymer patterning method has been described in our previous publication.³³ The polymer that we used in this work was polystyrene (PS, M_w 50k, PolyScience Inc.). Briefly, a PS film spun cast onto a single crystal ZnO (sc-ZnO) substrate (Semiconductor Wafer, Inc.) or a textured ZnO seed layer chemically grown on a Si substrate¹⁰ was approached by a fluorinated Si stamp containing 2D conical-shaped sharp tip arrays, with a tip radius of <10 nm, tip length of $0.5\text{--}1.5$ μm , and periodicity of 2.12 μm (Fig. 1). When the stamp gently touched the film surface by applying a mild pressure for tens of seconds, hollow circular patterns were formed simultaneously under the areas in contact with the stamp. In order to obtain appropriate hole size and well define the orientation of ZnO NWs grown from the substrate, the thickness of the PS film was controlled to be $50\text{--}80$ nm. Particularly, the 50 nm-diameter circular hole array was made by imprinting a freshly prepared 60 nm thick PS film at 60 $^\circ\text{C}$ under 3 bar pressure for 30 seconds. In order to control the NW diameter, subsequent thermal annealing was applied on the patterned PS film containing 50 nm holes at 75 $^\circ\text{C}$ for 15 and 30 s in air to tune the opening diameters to 100 and 300 nm. The accuracy we have reached in tuning the hole diameter by thermal annealing was about 5 nm.

Growth of ZnO NWs

The ZnO NW arrays were synthesized in the nutrient aqueous solution of 20 mmol L^{-1} $1:1$ zinc nitrate hydrate ($\text{Zn}(\text{NO}_3)_2 \cdot x\text{H}_2\text{O}$)

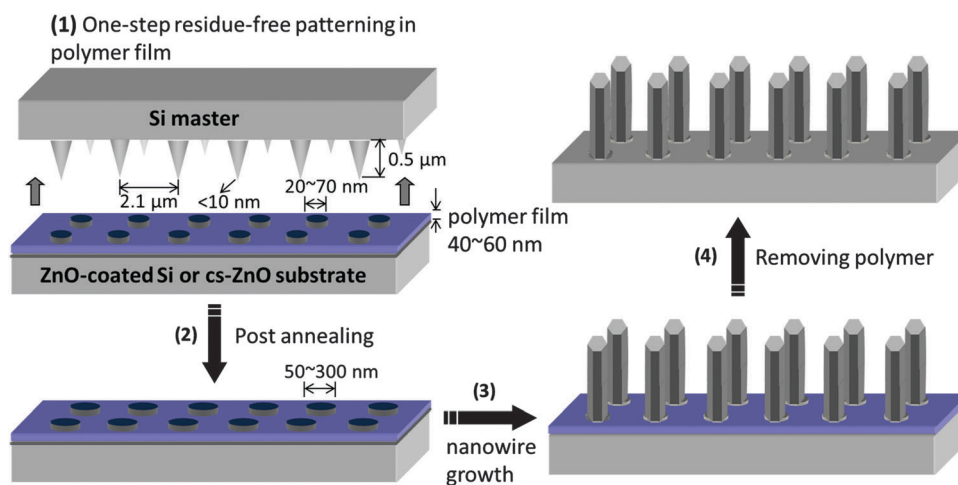


Fig. 1 Schematic of the fabrication of 2-D patterned well-aligned ZnO NW arrays. (1) A $40\text{--}60$ nm thick polymer film, spun cast on the ZnO substrate, is approached by a fluorinated Si stamp containing conical-shaped sharp tip arrays, with a tip radius of <10 nm, tip length of 0.5 μm , and periodicity of 2.1 μm . The stamp gently touches the film surface by applying a pressure of $3\text{--}5$ bar. A $20\text{--}70$ nm diameter circular opening array forms under the areas in contact with the stamp. After $50\text{--}60$ seconds, the stamp is lifted from the film. (2) The diameter of the as-produced openings in the polymer film was increased from 50 to 100 and 300 nm by using thermal annealing at 75 $^\circ\text{C}$. (3) Growth of single ZnO NWs by hydrothermal synthesis. (4) Removal of the polymer film by soaking the sample in a solvent.

and hexamethylenetetramine (HMTA). The substrates were vertically placed in the nutrient solution. The whole system was heated in a water bath up to 96 °C for 20 and 120 minutes respectively for growing the 0.65 and 3.2 μm long NWs.

Morphology and crystal structure characterization

The morphologies of the as-produced ZnO NW arrays were studied by SEM (Variable pressure, Leo) and AFM (Molecular Force Probe MFP-3D, Asylum Research) under tapping mode. The crystal structures of the ZnO NWs were studied by TEM and XRD (Philips/Panalytical PW3050/65 X'Pert). TEM samples were prepared by transferring the as-grown ZnO NWs to a carbon film on a copper grid. A Phillips CM30 microscope, equipped with a LaB6 thermionic gun and a 300 keV acceleration voltage, was used to perform conventional TEM including bright field, dark field and diffraction on individual ZnO NWs.

Electrical property characterization

The morphology and piezoelectric properties of the as-produced ZnO NW arrays were studied by using the conducting AFM (Molecular Force Probe MFP-3D, Asylum Research) with a Pt/Ir-coated Si probe (tapping probe, probe tip height: 10–15 μm , tip radius of curvature: 10–20 nm, cantilever: Si, resistivity: 0.01–0.02 $\Omega\text{ cm}$, resonance frequency: 204–497 kHz, spring constant: 0.1 N m^{-1} , nanosensors). The I - V spectra at contact

mode was recorded under dark conditions at a voltage sweep rate of 3 mV s^{-1} using a constant normal force of 6 or 8 nN. The piezoelectric responses *via* single NW manipulation or during AFM scanning at contact mode were measured without any external voltage. When the tip scanned over the top of the ZnO NWs, the position of the tip was adjusted according to the surface morphology and local contacting force. A metal pin fixed on the metal sample holder was used to fix the sample and connect the substrate to the measurement circuit for their electric contact. Silver paint was applied between the bottom of ZnO substrate and the sample holder to make sure a good electric contact. The electrode at the base of the sample was grounded. For single NW piezoelectricity measurements, multiple experiments (20–30 times) were performed with the cAFM cantilever tip pressing at all positions (position 1, 2, 3 and 4 as shown in Fig. 5) in order to investigate the repeatability and reliability of the cAFM piezoelectric experiments.

Results and discussion

Morphology of ZnO nanowires

Perfectly aligned and highly uniform ZnO NW arrays, as shown in Fig. 2, were successfully fabricated on sc-ZnO substrates using this approach, with each opening containing a single NW. The TEM images have shown very good crystallinity and a close match

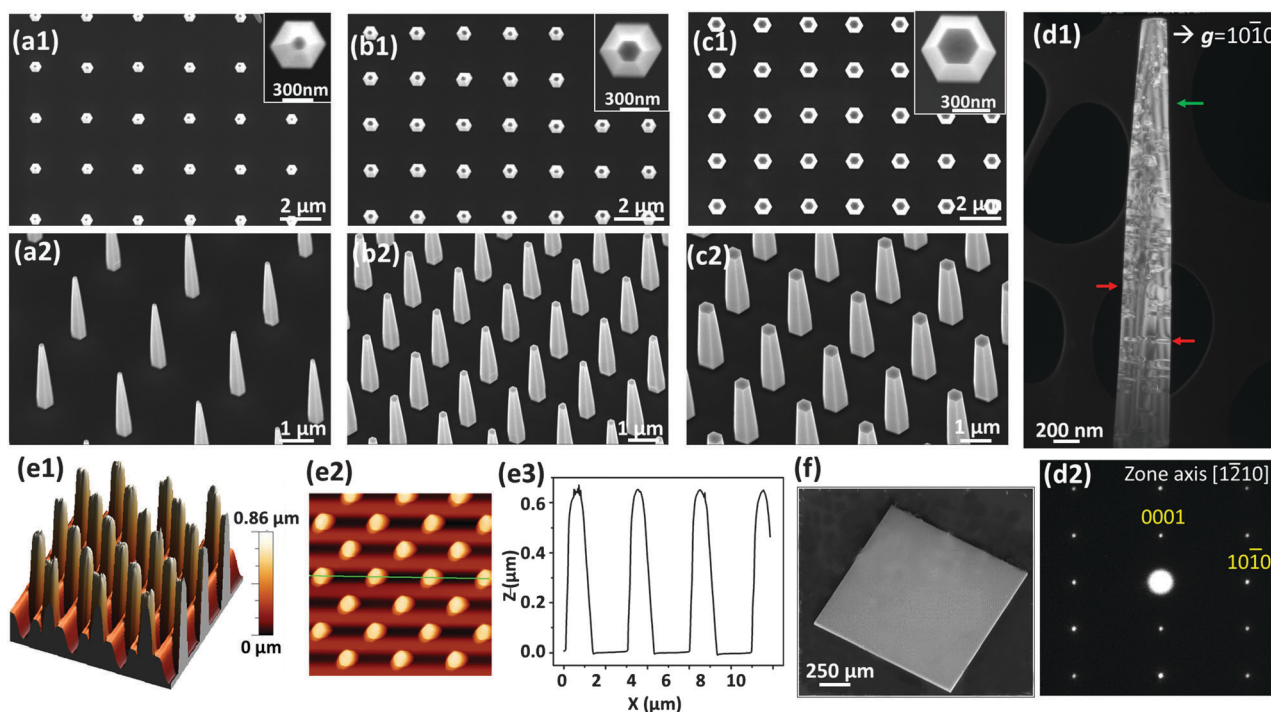


Fig. 2 SEM (a–c and f), TEM (d) and AFM (e) images of 2.12 μm pitch patterned nanowire arrays grown in 20 mmol L^{-1} nutrient aqueous solution for 20 minutes, on patterned ZnO crystal substrates. (a1)–(c1) are plane view images. Insets: magnified image of a single NW; (a2–c2) are 45° tilt view images, corresponding to (a1–c1). The opening diameters in (a), (b) and (c) are 50, 100 and 300 nm, respectively. (f) is the 45° tilt view panoramic SEM image of a 1 \times 1 cm patterned NW array, corresponding to (c1) and (c2). (d1) is a weak beam dark field TEM image of a NW grown identically for 120 minutes, with red arrows pointing out possible planar defects and green arrow the thickness fringes. Corresponding diffraction patterns taken on the zone axis $[1\bar{2}10]$ are shown in (d2), with two typical diffraction spots labeled. (e1–e3) are (tapping mode) AFM 3-D height image, plane-view height image, and cross-section profile of the NWs grown from 100 nm openings under identical conditions for 20 minutes.

between the (0001) crystal plane of the sc-ZnO substrate and the NW lattice. This is good proof of the fact that the polymeric materials were spontaneously excluded from the contact area during the stamping step, leaving a neat and clean substrate surface. Meanwhile, the polymer surrounding the hole formed a slightly elevated rim, provided effective spatial confinement to guide the NW growth. For comparison, ZnO NW arrays were also synthesized on ZnO seed layers deposited on Si substrates (Fig. S1, ESI†). Interestingly, the opening size affected the number of the as-prepared ZnO NWs grown from a single opening. Vertically aligned single NW was observed to grow out of 50 nm-diameter PS holes. On the other hand, multiple ZnO NWs were seen in holes with 100 and 300 nm openings. The number of NWs was likely determined by the number of ZnO seeds exposed in each opening. Previous research has shown that when the accessible nucleation sites increased, denser but smaller ZnO NWs would form.³⁴ In our case, more ZnO seeds would be contained in larger PS holes, resulting in the phenomenon we observed (Fig. S1, ESI†). Appropriate treatment of the ZnO seed layer has been demonstrated to be able to control the density of ZnO NWs, which can be potentially applied in our method to produce single ZnO NWs.^{34,35}

Fig. 2a–c shows the top-view (Fig. 2a1–c1) and 45° tilted-view (Fig. 2a2–c2) SEM images of highly uniform ZnO NW arrays grown on sc-ZnO substrates. Thermal annealing of the nano-patterned PS film induced an expansion of the hole size due to the increased polymer chain mobility and removal of the remaining solvent.³³ As the opening size increased from 50 to 100 and 300 nm, the NW top diameters increased from 144 nm to 211 nm and 380 nm, respectively, and the bottom diameters from 400 nm to 560 nm and 600 nm; while the height remained the same at 3.2 μm for 120 minute growth and at 0.65 μm for 20 minute growth, as measured by AFM (Fig. 2e1–e3). Their shapes and sizes were very uniform, with only 0.8% standard deviation (STD) for their diameters, for example, in the case of the NWs grown from 300 nm openings. The result showed that both the hole size and the lateral growth of ZnO nanowires were highly uniform and reproducible. The NWs were regular hexagonal pillars with a uniform conical shape, whose diameter gradually decreased from the bottom to the top (approx. half of the bottom size). The top/bottom outer diameter of the NWs, grown from the 100 nm openings for example, was 211/560 nm, respectively. It should be noted that their diameters exceed the size of the openings in polymer films as a result of overgrowth in lateral directions.²⁸ Using the polymer mask, the NWs were placed with a minimal positional deviation of 0.9% (18 nm STD for the 2.12 μm pitch), calculated by measuring the center-to-center distance between the ZnO NWs (Fig. 2e1–e3). Additionally, the panoramic view image in Fig. 2f reveals that the area of uniformly aligned NWs can reach 1 × 1 mm², showing the excellent large-scale patterning capability of our method.

The TEM diffraction patterns (Fig. 2d2) indicate that the NWs are single crystalline with hexagonal symmetry, consistent with the wurtzite structure of ZnO. Together with the SEM images, we can infer that the NWs grow along the [0001] direction and are enclosed by six facets.³⁶ In the weak beam dark field image taken

with a reflection $g = 10\text{--}10$, we observe the thickness fringes along the NW, as shown by the green arrow in Fig. 2d1, which is due to the 2D projection of the crystal facet and indicates the good crystalline quality of the NWs. Planar defects are also observed, as pointed out by the red arrows in Fig. 2d1. The good morphology and crystallinity indicated that high-quality ZnO NWs were achieved during the synthesis and that the PS film, with a T_g of ~ 100 °C, survived the NW growth without deformation or decomposition. The ZnO NW fabricated on ZnO seed layer-covered Si generally showed the same structure/crystallinity as those obtained from the sc-ZnO substrate, with some slight differences in NW geometric parameters (Fig. S2, ESI†).

Characterization of piezoelectric properties

The semiconducting-piezoelectric dual properties are characteristic for ZnO NWs and required for many applications.⁵ It is highly desirable that the patterned NWs are able to yield stable and uniform piezoelectric output current over a large surface area. To characterize the piezoelectric properties of thus-prepared NW arrays, the electric responses to the mechanical deformation of the NW arrays were measured using cAFM. When the cAFM tip scanned across the as-grown ZnO NW array, the output current signals were simultaneously collected along with the height signals. The current was defined in such a way that positive current represented that the electrons moved from ZnO NWs to the AFM tip.³⁷ We observed regular current signals clearly registered to the NW location, as shown in Fig. 3. The output current was almost identical for all the NWs, indicating that the consistently high quality of individual nanowires led to uniform piezoelectric properties across the sample. The current signals were comparable to the (disordered) output signals from homogeneously grown ZnO NW arrays reported previously,^{37–39} but the uniform bending distance recorded in the topography image (Fig. 3a) was observed much more clearly.⁴⁰ From the output current, the ZnO NWs can be identified as n-type.^{28,37} The observed positive current was in line with theoretical studies on potential and electron distributions in bent ZnO NWs, where the charge carriers were accumulated at the stretched side of the ZnO NW, while the electrons at the compressive side were largely depleted.^{37,38}

It is important to note that, despite the good matching between the topography and current, the measurements given above and also in previous reports involved complicated movements of both the cAFM tip and NWs: as the cAFM tip scanned laterally across such high aspect-ratio features, sudden vertical movements of the scanner were required to maintain the constant contact force.^{37,39,40} Depending on the particular microscope used, this could induce both topographic and electrical artifacts. This inevitable problem, together with the complexity of the varying contact interface and mechanics in the lateral scan measurement, made the data analysis and explanation of the NW piezoelectric behavior complicated.⁴¹ To avoid scanning-related artifacts, we further vertically compressed individual ZnO NWs with a constant force or bias to investigate their electrical and piezoelectric properties, as illustrated in Fig. 4a. Since the

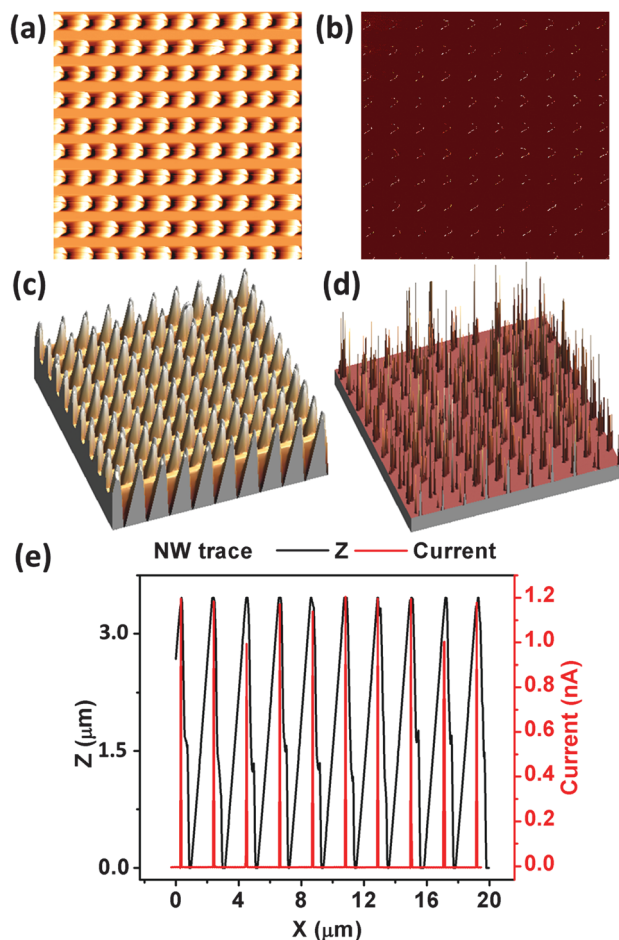


Fig. 3 Topographic (a and c) and current (b and d) images of NW arrays as shown in Fig. 2b2 in contact mode. The height and top diameter of the NWs are 3.2 μm and 250 nm, respectively. (c) and (d) are 3D images of (a) and (b) respectively. (e) shows the corresponding topographic and current profiles. Scan area: 20 μm . Scan speed: 25 $\mu\text{m s}^{-1}$. The AFM data were analyzed using WSxM 4.0.⁵²

measured current was produced without the interference from any lateral force as reported before,^{39,40} other complicating factors that might affect the analysis of the data, such as displacement current,⁴² changes in capacitance/resistance of the tip-sample contact, and triboelectric effect,⁴³ could be ruled out.

All the single NW characterizations were performed with 330 nm-wide (top diameter) and 3.2 μm -tall ZnO NWs. First, I - V curves of individual ZnO NWs were recorded (Fig. 4a). These I - V curves showed a typical Schottky contact behavior.⁴⁴ The rectifying behavior of the I - V curve indicated the existence of the Schottky barrier across the tip-nanowire, which was important for piezoelectric charge preservation.⁴⁵ From the I - V curves, we plotted $\ln|I| \propto |V|^{1/4}$,⁴⁶ and obtained a good linear relationship as shown in Fig. S3 (ESI[†]). This result verified that the piezoelectric potential was generated at the metal tip-semiconductor NW interface under external mechanical force, which had been known as piezotronic effect and utilized to fabricate strained piezotronic transistor arrays using vertical ZnO NWs.^{46,47} The very uniform and aligned ZnO arrays produced here are

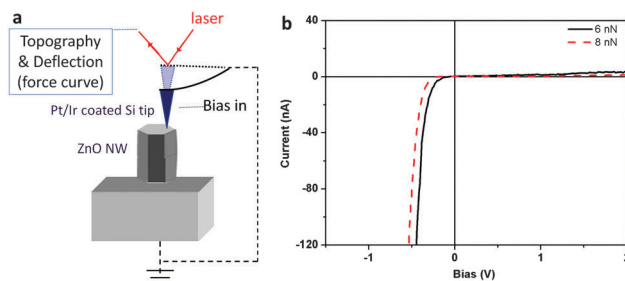


Fig. 4 (a) Schematics of the cAFM measurement on individual ZnO NW. (b) I - V curves obtained by aligning the AFM tip on the top of a ZnO NW (position 1) with the applied force of 6 and 8 nN respectively and bias sweeping a cycle between -2 and 2 V: starting from 0 to 4, back to 0, and then to -4 , finally back to 0 V. Rate: 3 mV s^{-1} .

expected to further improve the performance of such transistor arrays and their potential application in high-resolution strain and pressure mapping.

Based on this finding and using the same setup, we further studied the piezoelectric characteristics of single ZnO NWs in the way as illustrated in Fig. 5a, right panel. A cAFM tip was repeatedly brought into contact at different positions on the top of individual vertically aligned ZnO NWs without any applied bias. The current response and cantilever deflection upon vertically pressing at each position on the NW top surface illustrated in Fig. 5b were simultaneously recorded, as shown in Fig. 5c1-c4. All measurements were repeated for 100 cycles and the average data are presented with STDs in the range of 0.2–8%.

A control experiment was conducted on the substrate (position 0), with the AFM cantilever deflected by an identical amount as when on the top of a NW; no detectable current response (< 1 pA) was observed, as shown in Fig. 5c0, which is consistent with the fact that no piezoelectricity was generated. In contrast, a small amount of pA current was observed upon vertically pressing onto the center of the NW (position “1” as shown in Fig. 5c1). When the tip is pressed slightly off-center (38 nm, position “2”), a higher current was observed at the moment when the cantilever deflection was 46 nm, and the current increased to 46–68 pA (56 pA on average) at a deflection of 80 nm, which corresponds to an applied force of 8 nN. When the tip was moved further towards the edge, the current response increased to 95 and 136 pA, at positions “3” and “4”, 76 and 114 nm away from the NW center. Such vertical pressing at a series of different positions on the NW top surface with precise distances from the center resulted in well-controlled deflection of NWs. This was indicated by the different deflections of the cantilever under the same pressing force (Fig. 5c0-c4) and also previously observed from the bending distance recorded in the topography image (Fig. 3a). The generation of output current directly and clearly revealed the piezoelectricity of ZnO NWs, which was in agreement with a previous result obtained by laterally scanning across ZnO NWs.²⁸ The vertical loading generated dipoles in the bent NW, which in turn created a potential difference perpendicular to the axis of the NW. The clear position-dependence of output current we observed was attributed to the larger deformation of ZnO NW under an

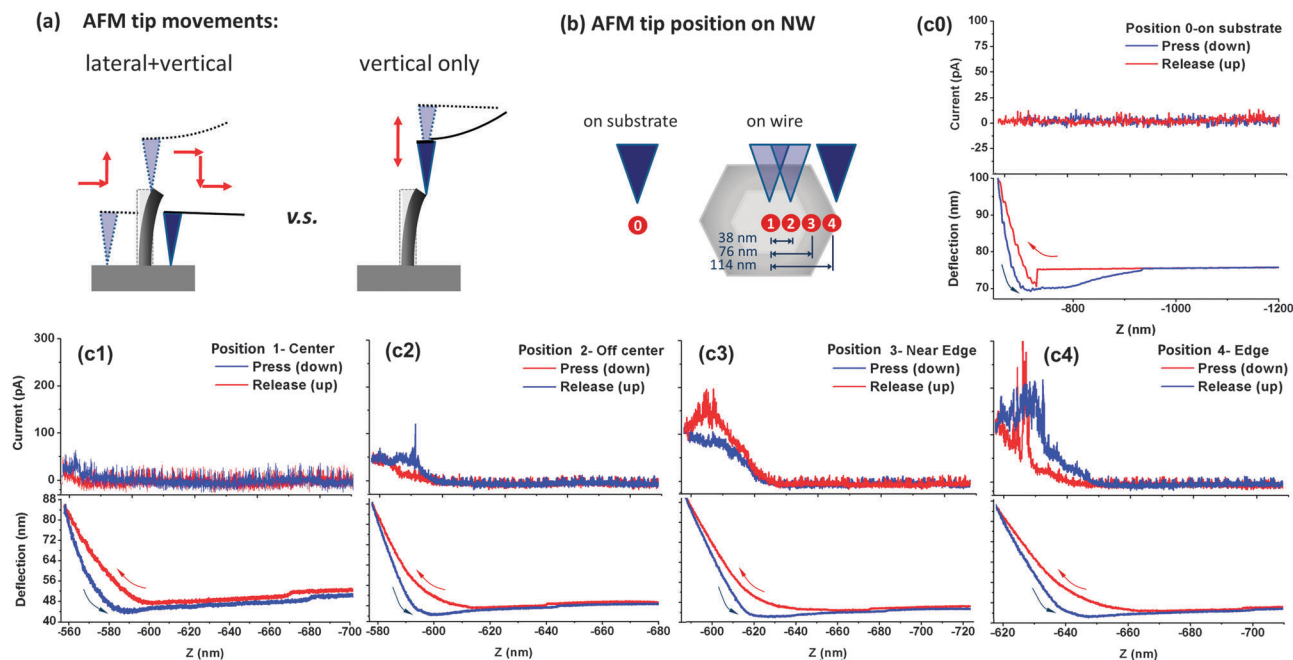


Fig. 5 (a) Schematics of single NW bending using cAFM. (b) Positions probed (c0–c4) current–force curves showing the current response (upper) and the deflection of cantilever (lower) as the function of vertical distance of the AFM tip. Recorded without bias applied, and while vertically pressing (red curves) and subsequently withdrawing (blue curves) away from the substrate at various positions (c0).

off-center force. Such a property is highly valued and may be applied in sensing, high-resolution strain, pressure mapping, *etc.* The statistical data for different positions at 80 nm deflection are summarized in Table S1 (ESI[†]). Our results can be rationalized by a simple calculation on the relationship of the piezoelectricity *versus* force applied on the center of the ZnO (see the ESI[†] for more details). Briefly, the piezoelectric effect came from a change in the dimension of the NW under compression (note, we assume a vertical compression for simplicity, rather than bending of the NW). By taking into account the Young's modulus, the aspect ratio of the NW, and the ZnO *c*-axis piezoelectric constant, we can plot the voltage output as a function of compressive force (Fig. S4, ESI[†]). The order of magnitude of the predicted voltage produced compares reasonably well with experimental data taken at 8 nN (after converting the current to voltage).

Conclusions

In conclusion, we have demonstrated how one-step residual-free nanopatterning in combination with hydrothermal synthesis under mild conditions can be used as a cost-efficient method to fabricate highly vertically aligned and uniform NW arrays with good positional and dimensional accuracy. As a proof-of-concept example, ZnO NWs with top diameters ranging from 144 nm to 300 nm and lengths from 0.65 to 3.2 μm were obtained with good crystallinity. The control over the geometric parameters and spatial distribution of ZnO NWs greatly facilitated the study of electromechanical properties of individual ZnO NWs using cAFM. Large-area scanning yielded

an output current pattern matching the vertical displacements of the AFM tip. Closer characterization of individual ZnO NWs revealed that the increase in the bending of the NW induced by compressive force applied on the NW resulted in an increase in the output current. The magnitude of the output current appeared to be related directly to the degree of NW bending determined by where and how hard the AFM tip pressed onto the NW. These comprehensive studies on synthesis, fabrication and characterization provide an ideal platform for further investigations into the fundamentals of many other types of 1-D materials and offer a route to the incorporation of NWs with desired electrical properties into a variety of devices.

The perfect uniformity of the patterned 1-D nanomaterials, in terms of the geometric shape, diameter, height and crystallinity, would lead to highly uniform physical properties and functions such as the bending induced current. Particularly, a consistent electric power generated by uniaxially compressing a highly aligned array of piezoelectric nanowires (*e.g.* ZnO, $\text{PbZr}_x\text{Ti}_{1-x}\text{O}_3$, *etc.*) of the same height prepared by this method would dramatically improve the feasibility and efficiency of using nanogenerators for powering mobile and even personal microelectronics.⁴⁸ Also, patterned and well-aligned high aspect-ratio nanostructures grown in this way allow the precise control of the interaction between incident light and microstructures and thus help improve optical function, such as the antireflection efficiency.⁴⁹ Controlling the spacing between nanostructures could solve the problem of insufficient infiltration of conjugated polymers into the nanostructured semiconducting matrix when fabricating hybrid polymer photovoltaic devices. These well-controlled arrays may serve as scaffolding for the deposition of other materials for an even wider range

of applications. Such in-site growth control can be applied to a broad range of materials, including metals, metal oxides and polymers. For example, PbSe nanorods and CuS nanowires have been synthesized *via* low temperature hydrothermal processes, which should be compatible with our method.^{50,51} This will aid the incorporation of nanomaterials into a variety of devices.

Acknowledgements

We thank Professor Zhonglin Wang (Georgia Institute Technology) for the valuable discussion and help with our calculations of the relationship between the piezoelectric voltage output and the compressive force applied on ZnO NWs.

Notes and references

- 1 Y. Cui and C. M. Lieber, *Science*, 2001, **291**, 851.
- 2 Y. Cui, X. Duan and C. M. Lieber, *J. Phys. Chem. B*, 2000, **104**, 5213.
- 3 H. J. Snaith, G. L. Whiting, B. Sun, N. C. Greenham, W. T. S. Huck and R. H. Friend, *Nano Lett.*, 2005, **5**, 1653.
- 4 X. Li, L. Basile, B. Huang, C. Ma, J. Lee, I. V. Vlassiuk, A. A. Poretzky, M. Lin, M. Yoon, M. Chi, J. C. Idrobo, C. M. Rouleau, B. G. Sumpter, D. B. Geohegan and K. Xiao, *ACS Nano*, 2015, **9**, 8078.
- 5 Z. L. Wang, *J. Phys.: Condens. Matter*, 2004, **16**, R829.
- 6 T. Makino, Y. Segawa, A. Tsukazaki, A. Ohtomo and M. Kawasaki, *Appl. Phys. Lett.*, 2005, **87**, 022101.
- 7 Ü. Özgür, Y. I. Alivov, C. Liu, A. Teke, M. A. Reshchikov, S. Doğan, V. Avrutin, S. J. Cho and H. A. Morkoç, *J. Appl. Phys.*, 2005, **98**, 041301.
- 8 P. Ravirajan, A. M. Peiró, M. K. Nazeeruddin, M. Graetzel, D. D. C. Bradley, J. R. Durrant and J. Nelson, *J. Phys. Chem. B*, 2006, **110**, 7635.
- 9 S. Yamabi and H. Imai, *J. Mater. Chem.*, 2002, **12**, 3773.
- 10 L. E. Greene, M. Law, D. H. Tan, M. Montano, J. Goldberger, G. Somorjai and P. Yang, *Nano Lett.*, 2005, **5**, 1231.
- 11 S. C. Rai, K. Wang, Y. Ding, J. K. Marmon, M. Bhatt, Y. Zhang, W. Zhou and Z. L. Wang, *ACS Nano*, 2015, **9**, 6419.
- 12 X. Wang, J. Song, J. Liu and Z. L. Wang, *Science*, 2007, **316**, 102.
- 13 Y. Qin, X. Wang and Z. L. Wang, *Nature*, 2008, **451**, 809.
- 14 J. Liu, S. Wang, Z. Bian, M. Shan and C. Huang, *Appl. Phys. Lett.*, 2009, **94**, 173107.
- 15 K. M. Coakley and M. D. McGehee, *Chem. Mater.*, 2004, **16**, 4533.
- 16 B. Kannan, K. Castelino and A. Majumdar, *Nano Lett.*, 2003, **3**, 1729.
- 17 X. He, F. Gao, G. Tu, D. Hasko, S. Hüttner, U. Steiner, N. C. Greenham, R. Friend and W. T. S. Huck, *Adv. Funct. Mater.*, 2011, **21**, 139.
- 18 H. Ng, J. Han, T. Yamada, P. Nguyen, Y. P. Chen and M. Meyyappan, *Nano Lett.*, 2004, **4**, 1247.
- 19 S. Xu, N. Adig, S. Ba, T. Desgupta, C. F. Wu and Z. L. Wang, *ACS Nano*, 2009, **3**, 1803.
- 20 X. He, F. Gao, G. Tu, D. Hasko, S. Hüttner, U. Steiner, N. C. Greenham, R. Friend and W. Huck, *Nano Lett.*, 2010, **10**, 1302.
- 21 J. Slota, X. He and W. Huck, *Nano Today*, 2010, **5**, 231.
- 22 A. I. Hochbaum, R. Fan, R. He and P. Yang, *Nano Lett.*, 2005, **5**, 457.
- 23 Y. Xia, P. Yang, Y. Sun, Y. Wu, B. Mayers, B. Gates, Y. Yin, F. Kim and H. Yan, *Adv. Mater.*, 2003, **15**, 353.
- 24 M. Huang, S. Mao, H. Feick, H. Yan, Y. Wu, H. Kind, E. Weber, R. Russo and P. Yang, *Science*, 2001, **292**, 1897.
- 25 M. Huang, Y. Wu, H. Feick, N. Tran, E. Weber and P. Yang, *Adv. Mater.*, 2001, **13**, 113.
- 26 W. Liu, F. Xiu, K. Sun, Y. H. Xie, K. L. Wang, Y. Wang, J. Zou, Z. Yang and J. L. Liu, *J. Am. Chem. Soc.*, 2010, **132**, 2498.
- 27 J. Zhang, L. D. Sun, J. L. Yin, H. L. Su, C. S. Liao and C. H. Yan, *Chem. Mater.*, 2002, **14**, 4172.
- 28 J. J. Cole, X. Wang, R. J. Knuesel and H. O. Jacobs, *Nano Lett.*, 2008, **8**, 1477.
- 29 Y. Wei, W. Wu, R. Guo, D. Yuan, S. Das and Z. L. Wang, *Nano Lett.*, 2010, **10**, 3414.
- 30 K. S. Kim, H. Jeong, M. S. Jeong and G. Y. Jung, *Adv. Funct. Mater.*, 2010, **20**, 3055.
- 31 S. Xu, Y. Wei, M. Kirkham, J. Liu, W. Mai, D. Davidovic, R. L. Snyder and Z. L. Wang, *J. Am. Chem. Soc.*, 2008, **130**, 14958.
- 32 L. H. Kaplan and B. K. Bergin, *J. Electrochem. Soc.*, 1980, **127**, 386.
- 33 X. He, J. Winkel and W. T. S. Huck, *Adv. Mater.*, 2009, **21**, 2083.
- 34 J. Liu, J. She, S. Deng, J. Chen and N. Xu, *J. Phys. Chem. C*, 2008, **112**, 11685.
- 35 L. W. Ji, S. M. Peng, J. S. Wu, W. S. Shih, C. Z. Wu and I. T. Tang, *J. Phys. Chem. Solids*, 2009, **70**, 1359.
- 36 M. Orban and I. R. Epstein, *J. Am. Chem. Soc.*, 1987, **109**, 101.
- 37 S. S. Lin, J. H. Song, Y. F. Lu and Z. L. Wang, *Nanotechnology*, 2009, **20**, 365703.
- 38 Y. Gao and Z. Wang, *Nano Lett.*, 2009, **9**, 1103.
- 39 M. Lu, J. Song, M. Lu, M. Chen, Y. Gao, L. Chen and Z. L. Wang, *Nano Lett.*, 2009, **9**, 1223.
- 40 J. Song, X. Wang, E. Riedo and Z. L. Wang, *Nano Lett.*, 2005, **5**, 1954.
- 41 Y. W. Heo, L. C. Tien, Y. Kwon, D. P. Norton, S. J. Pearton, B. S. Kang and F. Ren, *Appl. Phys. Lett.*, 2004, **85**, 2274.
- 42 J. D. Jackson, *Classical Electrodynamics*, Wiley, Hoboken, 1999.
- 43 R. A. Serway and J. W. Jewett, *Principles of Physics*, Brooks/Cole, Boston, 2006.
- 44 J. Volk, T. Nagata, R. Erdélyi, I. Bársony, A. L. Tóth, I. E. Lukács, Z. Czigány, H. Tomimoto, Y. Shingaya and T. Chikyow, *Nanoscale Res. Lett.*, 2009, **4**, 699.
- 45 Z. L. Wang and J. H. Song, *Science*, 2006, **312**, 242.

- 46 W. Han, Y. Zhou, Y. Zhang, C. Y. Chen, L. Lin, X. Wang, S. Wang and Z. L. Wang, *ACS Nano*, 2012, **6**, 3760.
- 47 Z. L. Wang, *Adv. Mater.*, 2012, **24**, 1410.
- 48 S. Xu, B. J. Hansen and Z. L. Wang, *Nat. Commun.*, 2010, **1**, 93.
- 49 S. Xu, N. Adig, S. Ba, T. Desgupta, C. F. Wu and Z. L. Wang, *ACS Nano*, 2009, **3**, 1803.
- 50 J. Yang, C. Xue, S. H. Yu, J. H. Zeng and Y. T. Qian, *Angew. Chem.*, 2002, **114**, 4891.
- 51 Q. Lu, F. Gao and D. Zhao, *Nano Lett.*, 2002, **2**, 725.
- 52 I. Horcas, R. Fernández, J. M. Gómez-Rodríguez, J. Colchero, J. Gómez-Herrero and A. M. Baro, *Rev. Sci. Instrum.*, 2007, **78**, 013705.